J Nanopart Res (2020) 22: 132
https://doi.org/10.1007/s11051-020-04861-3

RESEARCH PAPER

Novel synthesis of $BiVO_4$ using homogeneous precipitation and its enhanced photocatalytic activity

Ahmed Helal · Said M. El-Sheikh · Jianqiang Yu · Alaa I. Eid · S. A. El-Haka · S. E. Samra

Received: 30 January 2020 / Accepted: 23 April 2020 / Published online: 19 May 2020

Abstract The improvement of the photocatalyst performance with reducing the production cost is still the most important concern for finding target material properties and the possibility of mass production. Herein, we report a novel synthesis of $BiVO_4$ photocatalyst by homogeneous precipitation. Different surfactants such as polyvinylpyrrolidone (PVP), ethylene glycol (EG), cetyltrimethylammonium bromide (CTAB), and sodium dodecylbenzene sulphonate (SDBS) were added to assist the crystal orientation. XRD, SEM, Raman, and DRS were used to evaluate the crystal orientation of the as-synthesized $BiVO_4$ samples. The XRD revealed the purity of the produced samples except for SDBS that produced a mixture (tetragonal /monoclinic) phase. The Raman analysis confirmed that the PVP surfactant has the smallest V–O bond length that led to the lowest bandgap 2.17 eV. The photoelectrochemical results revealed that there is a decrease in the electron-hole recombination rate as shown from electrochemical impedance spectroscopy (EIS) data, as well as swelling of band pinning of the Fermi energy edge toward the negative direction according to the Mott-Schottky (MS) curve. These impacts are due to the different facets possessing truncated bipyramid-like shape which is created via PVP surfactant. These variations enhanced the photodegradation of methylene blue (MB) dye as a wastewater module.

Keywords $BiVO_4$ · Photocatalyst · MB photodegradation · Homogeneous precipitation · Nanostructured catalysts

This article is part of the topical collection: Nanotechnology in Arab Countries, Guest Editor: Sherif El-Eskandarany

Highlights
- Homogeneous precipitation is an effective and novel method to synthesize $BiVO_4$ photocatalyst.
- The electron carrier densities/electron transfer rate enhancement approved by Mott-Schottky
- The decreasing of (e–) and (h+) recombination confirmed by photoelectrochemical impedance (EIS).
- The $BiVO_4$ homojunction with different facets is an efficient for degradation of methylene blue.

A. Helal · S. M. El-Sheikh (✉) · A. I. Eid
Nanostructured Materials and Nanotechnology Division, Central Metallurgical Research and Development, Institute (CMRDI), P. O. 87 Helwan, Cairo 11421, Egypt
e-mail: selsheikh2001@gmail.com

A. Helal (✉) · J. Yu
Institute of Green Chemistry & Industrial Catalysis, School of Chemistry and Chemical Engineering, Qingdao University, Qingdao 266071, China
e-mail: ahelal31@yahoo.com

S. A. El-Haka · S. E. Samra
Department of Chemistry, Faculty of Science, Mansoura University, Mansoura, Egypt

Introduction

Environmental pollution is one of the most significant global issues due to the prominent growth of organic pollutant emissions in wastewater (Zhang et al. 2015). A variety of techniques for the removal of organic pollutants have been developed (Zhang et al. 2018).

Semiconductor-based heterogeneous photocatalysis has grabbed worldwide care due to its application in solar energy conversion and degradation of organic pollutants (Wu et al. 2018). Bismuth vanadate ($BiVO_4$) as a promising semiconductor showed interesting physicochemical properties including ferroelasticity, ionic conductivity, and acousto-optical photocatalytic activity (Kohtani et al. 2003; Zhao et al. 2010). Therefore, it has recently been applied in different applications such as gas sensors devices, posistors, solid-state electrolytes, lithium batteries, and lead-free paints as a yellow pigment (Shantha and Varma 1999). Also, it is an excellent material in the field of visible light–driven photocatalysts (Sayama et al. 2003)(Long et al. 2008)(Luo et al. 2008). It revealed an excellent photocatalytic H_2 production (Sayama et al. 2006) and O_2 evaluation form aqueous solution (Huang et al. 2017). Likewise, it demonstrated a good result for decontaminated wastewater from the organic material (Zhou et al. 2011). It photodegraded up to 90% methyl orange dye (MO) in 30 min under visible light irradiation (Zhou et al. 2006). Similarly, it exhibited a remarkable photoactivity of about 84% photodegraded for RhB dye (Tan et al. 2013). Also, It displayed a good photodecomposition about 93% of MB (Zhang et al. 2012). On the other hand, it gave a highly efficient degradation of 85% of phenol and 100% for trichlorophenol (Golmojdeh and Zanjanchi 2012). The activity of $BiVO_4$ is powerfully associated with its crystallinity and morphology. Meanwhile, it existed in three polymorphs, monoclinic scheelite, tetragonal zircon, and tetragonal scheelite. The monoclinic scheelite structure has the most reactive phase with direct bandgap of ~ 2.4–2.5 eV at ambient temperature (Walsh et al. 2009). Nevertheless, the pure monoclinic $BiVO_4$ still had low activity in the visible light range, (Yan et al. 2015) due to high electron-hole recombination which causes a diminutive lifetime of photogenerated electrons, low electrical conductivity, and poor hole transfer kinetic for water oxidation (Long et al. 2006). Numerous techniques have described synthesizing $BiVO_4$ in both bulk and thin film, for example, solid-state reaction (Zhong et al. 2011), aqueous solution method (Pilli et al. 2011), co-precipitation (Song Baia 2010), solvothermal (Wu et al. 2016), molten salt method (Liu et al. 2010), microwave irradiation (Zhang et al. 2008), and metal-organic decomposition (Galembeck and Alves 2002). These methods are used to prepare $BiVO_4$ with different shapes. In the ordinary precipitation process, the $BiVO_4$ was produced by adding ammonia directly to the metal cation solutions. This technique gave a slight control to the shape and size of precipitated particles due to the rapid rise of reaction pH (Fan et al. 2011). There is another method suitable for metal oxides precipitation called homogeneous precipitation. The significant feature of this method is greatly uniform precipitation carried out by the slow rise in the pH of the reaction mixture which is achieved by thermal decay of urea. This occurred when urea has been dissolved into an acidic media of a metal source and heated to about 90 °C; urea decays gradually due to the discharge of ammonia and carbonate ions into the acid media. This procedure produced a regular and uniformly insoluble metal oxide (Pookmanee et al. 2012). The homogeneous precipitation process was used previously to synthesize TiO_2 (Seo and Kim 2003), Al_2O_3 (Yasui 1988), $MgAl_2O_4$ (Meshkani and Fateme 2017), and Fe_3O_4 (Chen et al. 2010). Therefore, our research target of this report is to examine this technique as a novel procedure to synthesize the monoclinic $BiVO_4$. Different surfactants investigated to improve the morphology, band position, electron mobility, and electron-hole separation. Different electro-chemical techniques are used to prove the enhancement of optical properties of these materials such as impedance spectroscopy (EIS) and Mott-Schottky (MS) curve. This work extended for degradation of methylene blue. The obtained results revealed that the $BiVO_4$ homojunction with different facets is an efficient for degradation of methylene blue as model of textile wastewater compared with the previous published work.

Experimental part

Materials

Bismuth (III) nitrate pentahydrate Bi $(NO_3)_3{\cdot}5H_2O$ and ammonium metavanadate (NH_4VO_3) were used as a source for Bi and V, respectively; PVP, EG, CTAB, SDBS were used as orienting agents while urea has been employed as a precipitating agent. MB has been tested as a wastewater module to evaluate the photocatalytic activity of the existing photocatalysts. All used chemicals were analytical grade and they were obtained from Sinopharm Chemical Reagent Co., Ltd. (China).

Homogeneous precipitation of $BiVO_4$

Firstly, solution A: 0.24 mol/l Bi $(NO_3)_3$ $5H_2O$ in 100 ml of 2 M nitric acid and solution B: 0.24 mol/l NH_4VO_3 in 100 ml of 2 M nitric acid were prepared. After completely dissolving the precursor, the two solutions were mixed together by stirring for 30 min. Then, PVP, EG, CTAB, and SDBS were used as the orienting agent. Then, the mixture was transferred to the round flask that includes 0.3 M of urea heated at 90 °C and held there for 20 h to neutralize the reaction mixture and complete the precipitation. The yellow produced powder was washed with distilled water five times and one time with ethanol in a centrifuge. Then, the precipitate was dried at 90 °C for 24 h in a drying oven.

Characterization of the $BiVO_4$ photocatalysts

X-ray diffraction (XRD) patterns of as-prepared $BiVO_4$ samples were verified on a Bruker D8-advance X-ray diffractometer using Cu Kα radiation $\lambda = 0.15478$ nm, 40 kv, 30 mA. All results were recorded at a 2θ range between 10 and 80°. The morphologies of as-synthesized $BiVO_4$ samples were observed by scanning electron microscopy (JSM-6390LV). The Raman patterns of samples were measured by a microprobe Raman (Thermo scientific, DXR 532 laser) device, with excitation wavelength at 532 nm.

The bandgap energy of the prepared photocatalysts was recorded at 200–800-nm wavelength using diffuse reflectance spectroscopy with a JASCO V-570 UV–vis spectrophotometer equipped with a Labsphere integrating sphere diffuse reflectance accessory (Grätzel 1988). The diffuse reflectance mode (R) was recorded and transformed to the Kubelka-Munk function F(R) to separate the extent of light absorption from scattering light. Furthermore, the bandgap energy was calculated from the plot of the modified Kubelka-Munk function ($F(R)E^2$) versus the energy of the absorbed light E, according to the formula as follows (Tauc et al. 1966).

$$F(R)\,E^2 = \left(\frac{(1-R)^2}{2R} \times h\upsilon\right)^2 \quad (1)$$

A spectrofluorophotometer (RF-5301 PC, Japan, SHIMADZU) was used to measure the photoluminescence (PL) of the produced samples with excitation wavelength 365 nm.

Photocatalytic efficiency and photoelectrochemical performance

The photocatalytic activity was carried out by irradiation of the MB solution includes $BiVO_4$ photocatalyst using XPA-7 type photochemical reactor (Xujiang Machine Factory, Nanjing, China) attached by 800-W Xenon lamp with a 420-nm cut-off filter. The light intensity on each quartz tube equals 12.7 mW/cm. A water-cooling circulation system was established to preserve a constant reaction temperature. 0.04 g of our photocatalyst was blended with 40 ml MB [1 g/L] solution in a quartz reactor. Before the photocatalytic degradation, the solution was incubated under stirring and far from the light at room temperature for 60 min to neglect the amount of dye adsorped. The MB absorbance after complete adsorption was recorded to be the original concentration (C_o). Two milliliters of the reaction solution was taken from the upper part of the photoreactor at interval times followed by filtration through nylon syringe filters. The concentration of samples (C)$_t$ was measured immediately after separation using a MAPADA spectrophotometer. The photocatalytic efficiency of produced samples for photodegradation of dye was calculated by Eq. 2 (Khedr et al. 2017):

$$\%\text{photocatalytic degradation} = (1\text{-}C_t)/C_o \times 100 \quad (2)$$

The photoelectrochemical properties of as-prepared samples were estimated with the help of an electrochemical tester (CHI760E, Chenhua Instruments) with a typical three-electrode system. Our samples coated on fluorine-doped tin oxide (FTO) and used as a working electrode, the other electrodes used during measurement were Pt slice (2.0 × 2.0 cm) as a counter electrode while a saturated Ag/AgCl electrode was employed as a reference electrode, separately. Typically, 40 mg of sample was sonicated into 1 mL of Triton X-100 mixing with 1 mL acetylacetone and 1 ml ethyl alcohol under grinding to obtain a slurry, followed by further spread onto FTO with dimensions 1.0 × 1.0 cm. The prepared photoanodes were fixed at 200 °C for 2 h. A mixture solution of 0.5 mol/L Na_2SO_4 and 0.1 mol/L Na_2SO_3 was exploited as the electrolyte media. A 500-W Xenon lamp through a 420-nm cut-off filter was used as a visible light source (Peng et al. 2018).

Results and discussion

Crystal structure

Figure 1, displays the XRD patterns of produced $BiVO_4$ with different surfactants (surfactant-free, SDBS, CTAB, EG, and PVP). The XRD patterns of produced samples exhibited diffraction peaks defined as monoclinic $BiVO_4$ (JCPDS card no. 14-0688). SDBS-assisted $BiVO_4$ showed a diffraction peak indexed as the mixed-phase from the monoclinic and tetragonal phase (JCPDS card no. 14-0133). Additionally, no diffraction lines corresponding to any unreacted material such as Bi_2O_3 or other organic compounds related to surfactants were detected. These results show that the residual surfactant was removed without calcination. Also, it can be noticed that the 2θ peak positions of diffraction lines for the produced samples shifted in some manner. For example, 2θ at 28.5° and 30.5° revealed that EG- and PVP-assisted BiVO4 samples exposed an apparent shift to a lower angle compared with the surfactant-free sample. This indicates that there are some strain or distortion of the lattice (Shawky et al. 2019), and using EG and PVP as surfactants has a great influence on the crystal orientation of $BiVO_4$ during the homogeneous precipitation technique. This impact is due to the different molecular structures of each surfactant. Moreover, the diffraction peak at 2θ at 19° showed more splitting with the PVP-assisted $BiVO_4$ sample indicating the enhancement of the monoclinic crystallization phase (Zhu et al. 2013).

These observations are also clearly explained by the Raman technique that revealed more information about the bond structure of the prepared samples. The Raman bands in the range between 100 and 1000 cm^{-1} of $BiVO_4$ are prepared with different types of surfactants as shown in Fig. 2. From this Figure, it can be seen that the bands which appear to be around 324, 367 cm^{-1} are associated with the distortion of VO_4^{3-} tetrahedron and the asymmetric stretching vibration of the shorter V–O bond while Raman stretches around 710 and 811 cm^{-1} gave data about the V-O bond lengths. Moreover, as we see that the band position for a surfactant-free sample near 815 cm^{-1} was slightly shifted to 8.14.9, 812.97, and 810.08 for CTAB, EG, and PVP, respectively. This attributed to different degrees of distortion in V–O length of symmetry of the VO_4 tetrahedral. Also, it revealed that the lowest V–O bond length was obtained in the case of PVP which leads to a decrease in the length between the valence band and the conduction band (Thalluri et al. 2013). This result well matched with the XRD pattern shift.

FE-SEM images of the synthesized $BiVO_4$ samples with a different type of surfactant were depicted in Fig. 3. Figure 3a shows an agglomerated and irregular polyhedral microcrystal, with random size distributions in the range of 0.2–2 μm of the surfactant-free $BiVO_4$ sample. When the EG was used as surfactant, the

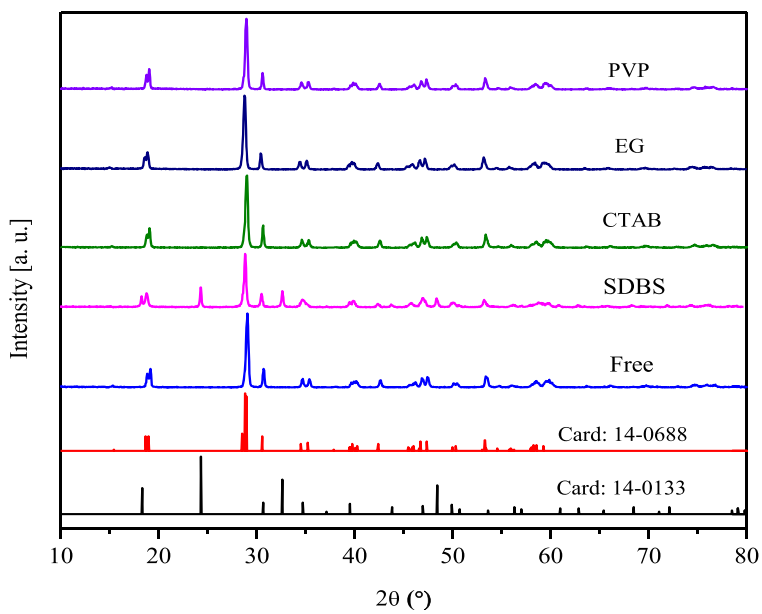

Fig. 1 XRD patterns of $BiVO_4$ photocatalysts prepared with different surfactants

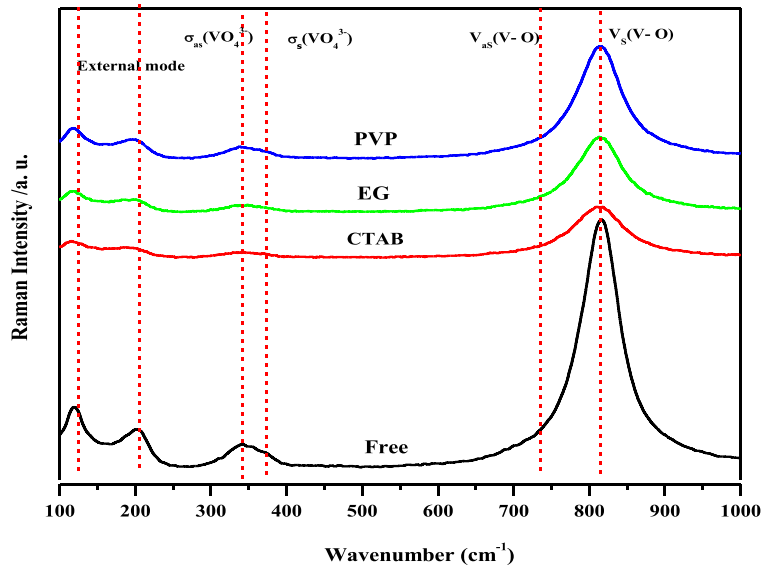

Fig. 2 Raman spectra of $BiVO_4$ sample fabricated using various surfactants

morphology of $BiVO_4$ completely changed from agglomerated and irregular polyhedral microcrystal to stacked platelets as displayed in Fig. 3b. On the other hand, when CTAB used as a surfactant, the morphology of $BiVO_4$ becomes irregular rods with aspect ratio 0.05 (width of 0.1 μm and length about 2 μm) as seen in

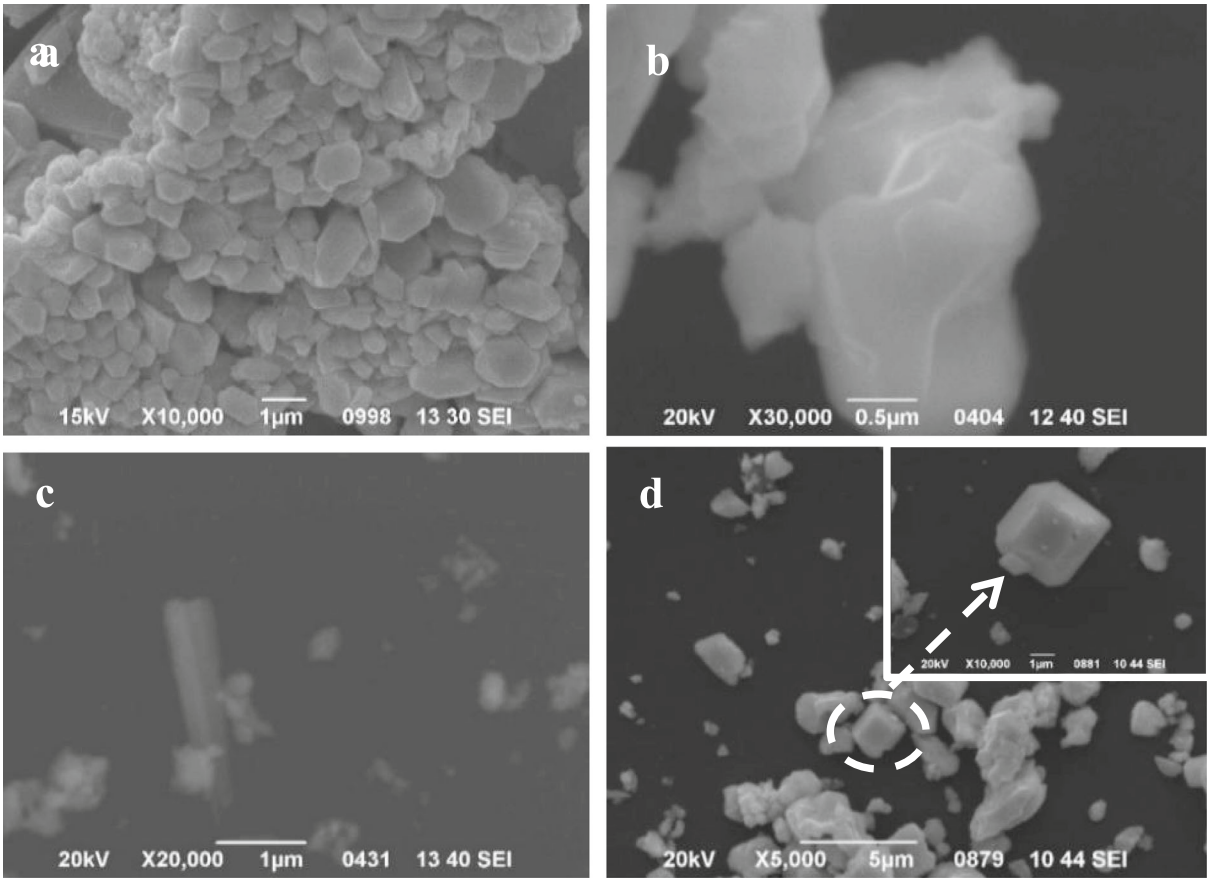

Fig. 3 SEM images for morphology of $BiVO_4$ sample fabricated with various surfactants

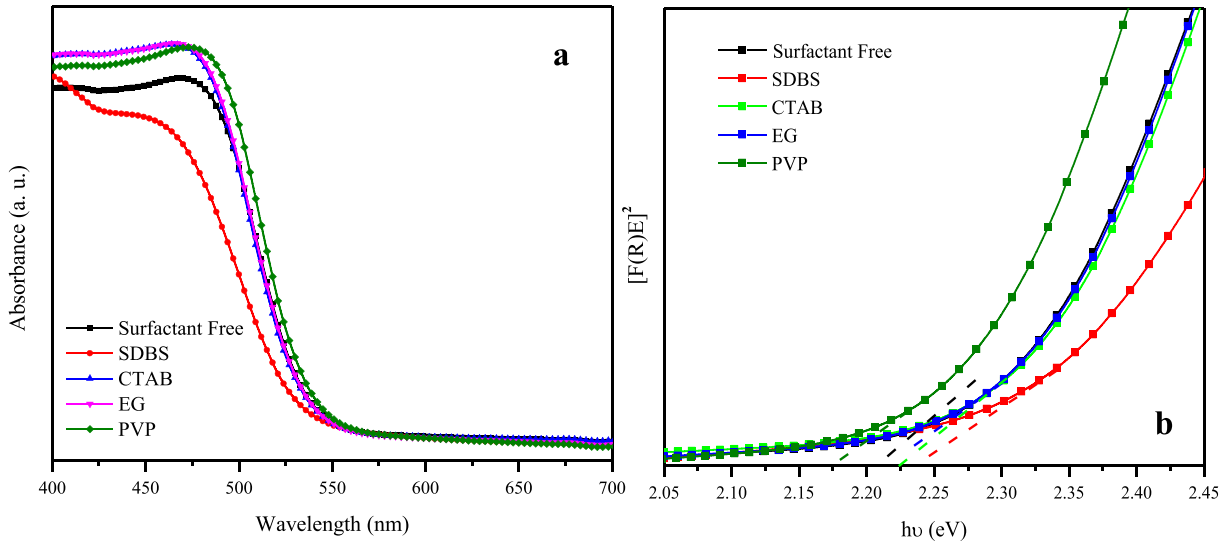

Fig. 4 **a** DRS spectra of $BiVO_4$ samples with different type of surfactant. **b** Plot of transferred Kubelka-Munk vs. energy of the light absorbed

Fig. 3c. Moreover, the influence of PVP surfactant on the morphology of $BiVO_4$ showed a truncated bipyramid-like shape and enlarged as seen in Fig. 3d. Inset in Fig. 3d revealed the image with different facets and relatively sharp edges with smooth surfaces characterized by "surface heterojunction" (Yu et al. 2014). In addition, this shape has a spatially photogenerated electron and hole separation onto its different facets which can improve the photocatalytic process (Li et al. 2014).

Optical properties, charge separation at different surfactant

DRS of prepared samples using different types of surfactants is shown in Fig. 4a. We can notice from this Figure, the $BiVO_4$ sample prepared using SDBS surfactant shows absorbance less than other samples related to the presence of tetragonal phase which subsequently has optical activity less than monoclinic (Fu et al. 2005).

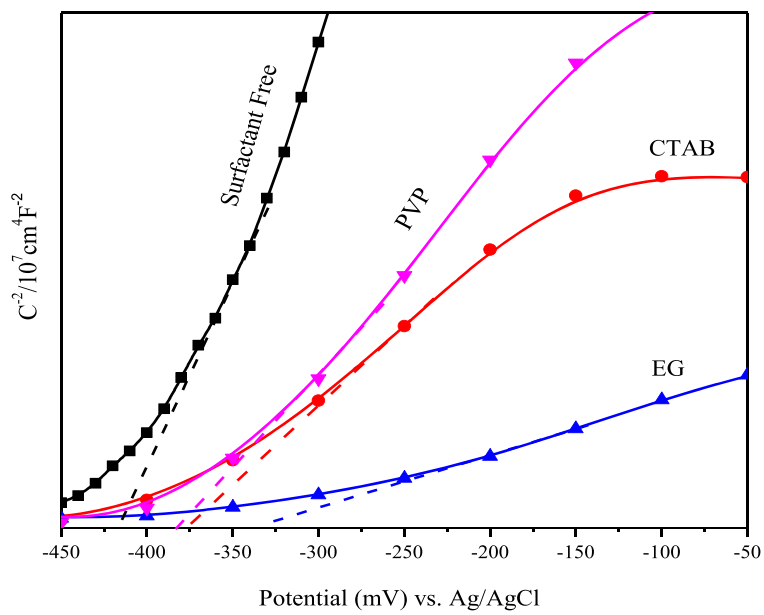

Fig. 5 Variation of capacitance (C) with the applied potential in presented in the Mott-Schottky relationship for the $BiVO_4$ samples with different surfactant

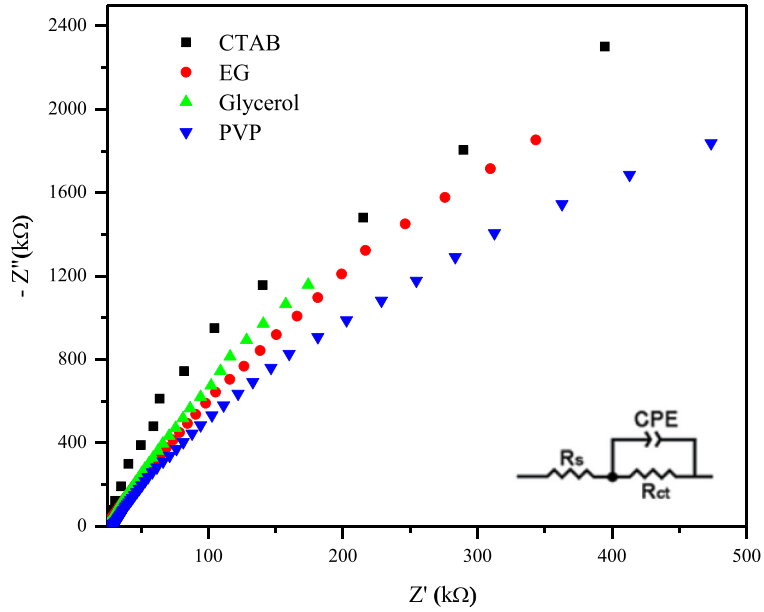

Fig. 6 Electrochemical impedance spectra of the $BiVO_4$ samples electrolyte. The equivalent circuit (inset)

Other samples showed enhancement in the absorbance with a slight redshift in the case of PVP. The bandgap (Eg) of synthesized samples has been calculated from the modified Kubelka-Munk function $[F(R)E]^2$ curves against the absorbed light energy E_g as shown in Fig. 4b. The E_g showed that the measured bandgaps of samples were 2.17, 2.20, 2.21, 2.22, and 2.24 eV for samples PVP, surfactant-free, EG, CTAB, and SDBS, respectively. From these results, PVP-assisted $BiVO_4$ sample shows the lowest bandgap, which refers to the minimum energy and band level, and predicts to increase the absorption through the visible light rays. To focus on the electronic structure, electron-hole separation process and the influence of surfactant, which improve the electron-hole recombination into $BiVO_4$ crystal (Abdellatif et al. 2012), Mott-Schottky (MS) and electrochemical impedance spectroscopy (EIS) curves of the synthesized samples are performed in the present study. MS curves of $BiVO_4$ samples displayed positive slopes as expected for *n*-type semiconductors Fig. 5. The flat band potential (intercept on the *x*-axis) is positively shifted after adding the surfactants, which is attributed

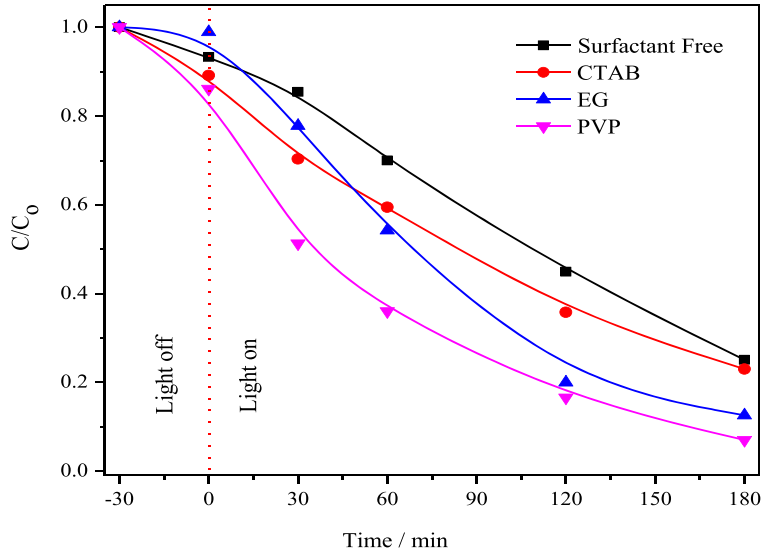

Fig. 7 Photodegradation efficiencies of MB as a function of irradiation time for different photocatalysts

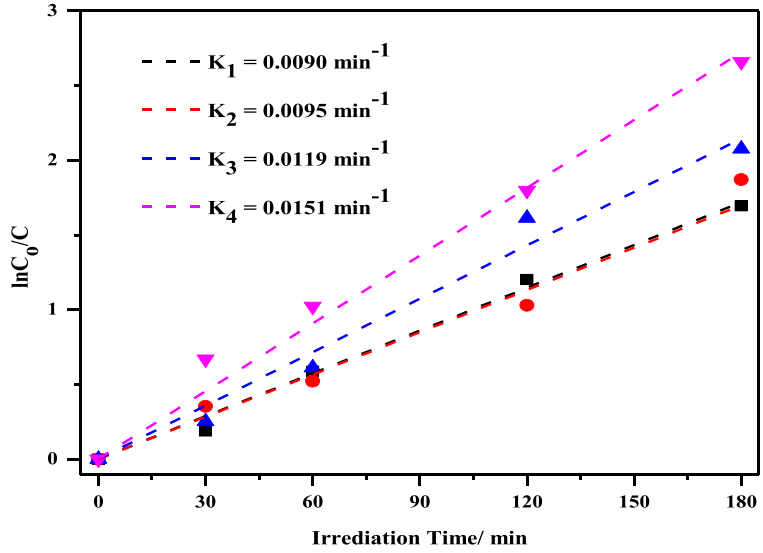

Fig. 8 MB photodegradation kinetics curves by $BiVO_4$ samples prepared with K_1: surfactant free, K_2: CTAB, K_3: ethylene glycol, K_4: PVP

to the swelling of the band pinning of the Fermi energy edge (Lv et al. 2017). On the other hand, the markedly shallower slope for $BiVO_4$ samples assisted by surfactants implying an increase of electron carrier densities and the electron transfer rate (Wang et al. 2013). Moreover, Fig. 6 exposed the electrochemical impedance spectroscopy (EIS) of prepared samples according to the corresponding circuit model (inset in Fig. 6), where R_s and R_{ct} were denoted to the series resistance and interfacial charge transfer resistance, respectively (Lv et al. 2017). Due to the similarity of the series resistance effect the value of R_s for all samples was neglected. After adding the surfactant, R_{ct} decreased significantly especially in PVP-assisted $BiVO_4$, suggesting that the presence of PVP greatly enhances charge transfer into the bulk material and at the sample || electrolyte interface. These results approve that the presence of surfactant especially PVP increases the electron-hole separation and electron mobility properties (Mao et al. 2014).

Photoactivity of $BiVO_4$ photocatalysts

The photoactivity performance of obtained samples synthesized with different surfactants is examined for the photodegradation of MB as shown in Fig. 7. From this Figure, we can observe the reduction in the concentration of MB using $BiVO_4$ photocatalysts during visible irradiation time. The photocatalytic activity of the $BiVO_4$ samples obtained with various surfactants much higher than that of synthesized surfactant-free $BiVO_4$. Compared with the photodegradation of 70% surfactant-free-$BiVO_4$, the efficiency of photo-degradation with PVP assisted $BiVO_4$ powder is up to 95% after

Table 1 Comparison between recent $BiVO_4$-based systems for MB photodegradation

Method	Application	Activity	Time	Phase	Ref.
microwave	MB degradation	75%	3 h	m-$BiVO_4$	(Intaphong 2016)
Reverse-microemulsion	MB degradation	80%	4 h	m-$BiVO_4$	(Chen-Yang Chung 2010)
combustion synthesis	MB degradation	75	3 h	m-$BiVO_4$	(Jiang et al. 2008)
Flame-assisted synthesis	MB degradation	95	6 h	m-$BiVO_4$	(Castillo et al. 2010)
ammonia co-precipitation	MB degradation	100%	4 h	m-$BiVO_4$	(Yu et al. 2009)
Hydrothermal preparation	MB degradation	90%	5 h	m-$BiVO_4$	(Ma et al. 2015)
Microwave/hydrothermal method	MB degradation	80%	3 h	m-$BiVO_4$	(Zhu et al. 2013)
Homogenous precipitation	MB degradation	95%	3 h	m-$BiVO_4$	This work

180 min under visible light irradiation. Moreover, the values of reaction rate constants "*k*" as extracted from Fig. 8 confirmed its photocatalytic activity results. The PVP-assisted $BiVO_4$ shows the highest rate constant of reaction ($K_4 = 0.0151\ min^{-1}$). The photocatalytic activity of PVP-assisted $BiVO_4$ sample is ascribed to the truncated bipyramid-like shape which is characterized by different facets with a different activity. This shape shows diminishes in the electron-hole recombination and enhanced the carrier density which leads to enhance the efficiency of the catalytic activity. So, in the future, we should study the effect of PVP addition and the impact of the synthesized $BiVO_4$ on catalytic activity. A comparison between the current work and other monoclinic $BiVO_4$-based photocatalyst is summarized in Table 1. From this table, it appears that homogeneous precipitation technique with PVP as a surfactant achieved the photonic efficiency of the $BiVO_4$ photocatalyst for degradation of MB dyes.

Conclusion

In summary, we have successfully prepared for the first-time monoclinic $BiVO_4$ photocatalyst via simple homogeneous precipitation assisted by different surfactants as orienting agents. The characterization and photocatalytic experiment demonstrate that the presence of PVP surfactant as orienting agent showed the best results due to the formation of truncated bipyramid-like shape which appeared in different facets with different activities. This improvement is confirmed by photoelectrochemical measurements, such as Mott-Schottky (MS), which showed an enhancement of the electrons, carrier densities, and the electron transfer rate. Moreover, the photoelectrochemical impedance (EIS) confirmed the decrease of the electrons/holes recombination. This work extended to the degradation of methylene blue. The obtained results revealed that the $BiVO_4$ homojunction with different facets is efficient for the degradation of methylene blue as a wastewater module compared with the previously published work.

Funding information This work is financially supported by the Talented Young Scientist Program, Chinese Science and Technology; National Natural Science Foundation of China for Youths (No. 21407065, 21506079), Natural Science Foundation of Shandong Province (No. ZR2016BM08).

Compliance with ethical standards

Conflict of interest The authors declare that they have no conflict of interest.

References

Abdellatif MH, Song JD, Choi WJ, Cho NK (2012) In/Ga interdiffusion in InAs quantum dot in InGaAs/GaAs asymmetric quantum well. J Nanosci Nanotechnol 12:5774–5777. https://doi.org/10.1166/jnn.2012.6280

Castillo NC, Heel A, Graule T, Pulgarin C (2010) Flame-assisted synthesis of nanoscale, amorphous and crystalline, spherical BiVO4 with visible-light photocatalytic activity. Appl Catal B-Environ 95(3–4):335–347

Chen J, Qian Y, Wei X (2010) Comparison of magnetic-nanometer titanium dioxide / ferriferous oxide (TiO_2/Fe_3O_4) composite photocatalyst prepared by acid – sol and homogeneous precipitation methods. J Mater Sci:6018–6024. https://doi.org/10.1007/s10853-010-4685-z

Chen-Yang Chung C-H (2010) Reverse-microemulsion preparation of visible-light-driven nano-sized BiVO4. J Alloy Compd 502(1):L1–L5

Fan H, Wang D, Wang L, Li H, Wang P, Jiang T, Xie T (2011) Hydrothermal synthesis and photoelectric properties of $BiVO_4$ with different morphologies: an efficient visible-light photocatalyst. Appl Surf Sci 257:7758–7762. https://doi.org/10.1016/j.apsusc.2011.04.025

Fu H, Pan C, Yao W, Zhu Y (2005) Visible-light-induced degradation of rhodamine B by nanosized Bi_2WO_6. J Phys Chem B 109:22432–22439. https://doi.org/10.1021/jp052995j

Galembeck A, Alves OL (2002) Bismuth vanadate synthesis by metallo-organic decomposition: thermal decomposition study and particle size control. J Mater Sci 37:1923–1927. https://doi.org/10.1023/A:1015206426473

Golmojdeh H, Zanjanchi MA (2012) A facile approach for synthesis of $BiVO_4$ nano-particles possessing high surface area and various morphologies. Cryst Res Technol 47:1014–1025. https://doi.org/10.1002/crat.201200216

Grätzel M (1988) Heterogenous photochemical electron transfer. CRC Press, Baton Rouge

Huang CK, Wu T, Huang CW et al (2017) Enhanced photocatalytic performance of $BiVO_4$ in aqueous $AgNO_3$ solution under visible light irradiation. Appl Surf Sci 399:10–19. https://doi.org/10.1016/j.apsusc.2016.12.038

Intaphong P, Phuruangrat A, Pookmanee P (2016) Synthesis and characterization of BiVO4 photocatalyst by microwave method. Integrated ferroelectrics 175:51–58

Jiang H-q, Endo H, Natori H, Nagai M, Kobayashi K (2008) Fabrication and photoactivities of spherical-shaped BiVO4 photocatalysts through solution combustion synthesis method. J Eur Ceram Soc 28(15):2955–2962

Khedr TM, El-Sheikh SM, Hakki A et al (2017) Highly active non-metals doped mixed-phase TiO_2 for photocatalytic oxidation of ibuprofen under visible light. J Photochem

Photobiol A Chem 346:530–540. https://doi.org/10.1016/j.jphotochem.2017.07.004

Kohtani S, Koshiko M, Kudo A, Tokumura K, Ishigaki Y, Toriba A, Hayakawa K, Nakagaki R (2003) Photodegradation of 4-alkylphenols using $BiVO_4$ photocatalyst under irradiation with visible light from a solar simulator. Appl Catal B Environ 46:573–586. https://doi.org/10.1016/S0926-3373(03)00320-5

Li R, Han H, Zhang F, Wang D, Li C (2014) Highly efficient photocatalysts constructed by rational assembly of dual-cocatalysts separately on different facets of $BiVO_4$. Energy Environ Sci 7:1369–1376. https://doi.org/10.1039/c3ee43304h

Liu Y, Ma J, Liu Z, Dai C, Song Z, Sun Y, Fang J, Zhao J (2010) Low-temperature synthesis of $BiVO_4$ crystallites in molten salt medium and their UV-vis absorption. Ceram Int 36:2073–2077. https://doi.org/10.1016/j.ceramint.2010.06.003

Long M, Cai W, Cai J, Zhou B, Chai X, Wu Y (2006) Efficient photocatalytic degradation of phenol over Co_3O_4 /$BiVO_4$ composite under visible light irradiation. J Phys Chem B 110:20211–20216. https://doi.org/10.1021/jp063441z

Long M, Cai W, Kisch H (2008) Visible light induced photoelectrochemical properties of n-$BiVO_4$ and n-$BiVO_4$/p-Co_3O_4. J Phys Chem C 112:548–554. https://doi.org/10.1021/jp075605x

Luo H, Mueller AH, McCleskey TM et al (2008) Structural and photoelectrochemical properties of BiVO4 thin films. J Phys Chem C 112:6099–6102. https://doi.org/10.1021/jp7113187

Lv X, Nie K, Lan H, Li X, Li Y, Sun X, Zhong J, Lee ST (2017) Fe_2TiO_5-incorporated hematite with surface P-modification for high-efficiency solar water splitting. Nano Energy 32:526–532. https://doi.org/10.1016/j.nanoen.2017.01.001

Ma W, Li Z, Liu W (2015) Hydrothermal preparation of BiVO4 photocatalyst with perforated hollow morphology and its performance on methylene blue degradation. Ceram Int 41:4340–4347

Mao C, Zuo F, Hou Y, Bu X, Feng P (2014) In situ preparation of a Ti^{3+} self-doped TiO_2 film with enhanced activity as photoanode by N_2H_4 reduction. Angew Chem Int Ed 53:10485–10489. https://doi.org/10.1002/anie.201406017

Meshkani F, Fateme S (2017) Nickel catalyst supported on mesoporous $MgAl_2O_4$ nanopowders synthesized via a homogenous precipitation method for dry reforming reaction. Res Chem Intermed 43:545–559. https://doi.org/10.1007/s11164-016-2639-z

Peng Y, Liu Q, Zhang J, Zhang Y, Geng M, Yu J (2018) Enhanced visible-light-driven photocatalytic activity by 0D/2D phase heterojunction of quantum dots/nanosheets on bismuth molybdates. J Phys Chem C 122:3738–3747

Pilli SK, Furtak TE, Brown LD et al (2011) Cobalt-phosphate (Co-Pi) catalyst modified Mo-doped $BiVO_4$ photoelectrodes for solar water oxidation. Energy Environ Sci 4:5028–5034. https://doi.org/10.1039/c1ee02444b

Pookmanee P, Kojinok S, Phanichphant S (2012) Bismuth vanadate ($BiVO_4$) powder prepared by the sol-gel method. J Met Mater Miner 22:49–53

Sayama K, Nomura A, Arai T (2006) Photoelectrochemical decomposition of water into H_2 and O_2 on porous $BiVO_4$ thin-film electrodes under visible light and significant effect of Ag ion treatment. J Phys Chem B 110:11352–11360. https://doi.org/10.1021/jp057539+

Sayama K, Nomura A, Zou Z, Abe R, Abe Y, Arakawa H (2003) Photoelectrochemical decomposition of water on nanocrystalline $BiVO_4$ film electrodes under visible light. Chem Commun 2908:2908–2909. https://doi.org/10.1039/b310428a

Seo DS, Kim H (2003) Synthesis and characterization of TiO_2 nanocrystalline powder prepared by homogeneous precipitation using urea. J Mater Res 18:571–577

Shantha K, Varma KBR (1999) Preparation and characterization of nanocrystalline powders of bismuth vanadate. Mater Sci Eng B Solid-State Mater Adv Technol 60:66–75. https://doi.org/10.1016/S0921-5107(99)00021-5

Shawky A, Mohamed RM, Mkhalid IA, Youssef MA, Awwad NS (2019) Visible light-responsive Ag/$LaTiO_3$ nanowire photocatalysts for efficient elimination of atrazine herbicide in water. J Mol Liq 299:112163. https://doi.org/10.1016/j.molliq.2019.112163

Song Baia YX (2010) Some recent developments in surface and interface design for photocatalytic and electrocatalytic hybrid structures. Optoelectron Adv Mater Rapid Commun 4:1166–1169. https://doi.org/10.1039/b000000x

Tan G, Zhang L, Ren H, Wei S, Huang J, Xia A (2013) Effects of pH on the hierarchical structures and photocatalytic performance of $BiVO_4$ powders prepared via the microwave hydrothermal method. ACS Appl Mater Interfaces 5:5186–5193. https://doi.org/10.1021/am401019m

Tauc J, Grigorovici R, Vancu A (1966) Optical properties and electronic structure of amorphous germanium. Phys Status Solidi 15:627–637. https://doi.org/10.1002/pssb.19660150224

Thalluri SRM, Martinez-Suarez C, Virga A, Russo N, Saracco G (2013) Insights from crystal size and band gap on the catalytic activity of monoclinic $BiVO_4$. Int J Chem Eng Appl 4:305–309. https://doi.org/10.7763/IJCEA.2013.V4.315

Walsh A, Yan Y, Huda MN, al-Jassim MM, Wei SH (2009) Band edge electronic structure of $BiVO_4$: elucidating the role of the Bi s and V d orbitals. Chem Mater 21:547–551. https://doi.org/10.1021/cm802894z

Wang Y, Zhang Y, Tang J et al (2013) Simultaneous etching and doping of TiO_2 nanowire arrays for enhanced photoelectrochemical performance. ACS Nano 7:9375–9383. https://doi.org/10.1021/nn4040876

Wu D, Wang W, Ng TW, Huang G, Xia D, Yip HY, Lee HK, Li G, An T, Wong PK (2016) Visible-light-driven photocatalytic bacterial inactivation and the mechanism of zinc oxysulfide under LED light irradiation. J Mater Chem A 4:1052–1059. https://doi.org/10.1039/c5ta08044d

Wu M, Jing Q, Feng X, Chen L (2018) $BiVO_4$ microstructures with various morphologies: synthesis and characterization. Appl Surf Sci 427:525–532. https://doi.org/10.1016/j.apsusc.2017.07.299

Yan X, Li W, Aberle AG, Venkataraj S (2015) Surface texturing studies of bilayer transparent conductive oxide (TCO) structures as front electrode for thin-film silicon solar cells. J Mater Sci Mater Electron 26:7049–7058. https://doi.org/10.1007/s10854-015-3326-3

Yasui I (1988) Synthesis of hydrous SnO_2 and SnO_2-coated TiO_2 powders by the homogeneous precipitation method and their characterization. J Mater Sci 23:637–642

Yu J, Low J, Xiao W, Zhou P, Jaroniec M (2014) Enhanced photocatalytic CO_2-reduction activity of anatase TiO_2 by

Co-exposed {001} and {101} facets. J Am Chem Soc 136: 8839–8842

Yu J, Zhang Y, Kudo A (2009) Synthesis and photocatalytic performances of BiVO4 by ammonia co-precipitation process. Journal of Solid State Chemistry 182(2):223–228

Zhang G, Wurtzler EM, He X, Nadagouda MN, O'Shea K, el-Sheikh SM, Ismail AA, Wendell D, Dionysiou DD (2015) Identification of TiO_2 photocatalytic destruction byproducts and reaction pathway of cylindrospermopsin. Appl Catal B Environ 163:591–598

Zhang HM, Liu JB, Wang H, Zhang WX, Yan H (2008) Rapid microwave-assisted synthesis of phase controlled $BiVO_4$ nanocrystals and research on photocatalytic properties under visible light irradiation. J Nanopart Res 10:767–774. https://doi.org/10.1007/s11051-007-9310-y

Zhang K, Liu Y, Deng J, Xie S, Zhao X, Yang J, Han Z, Dai H (2018) Co–Pd/$BiVO_4$: high-performance photocatalysts for the degradation of phenol under visible light irradiation. Appl Catal B Environ 224:350–359. https://doi.org/10.1016/j.apcatb.2017.10.044

Zhang L, Long J, Pan W (2012) Efficient removal of methylene blue over composite-phase $BiVO_4$ fabricated by hydrothermal control synthesis. Mater Chem Phys 136:897–902. https://doi.org/10.1016/j.matchemphys.2012.08.016

Zhao Z, Luo W, Li Z, Zou Z (2010) Density functional theory study of doping effects in monoclinic clinobisvanite $BiVO_4$. Phys Lett Sect A Gen At Solid State Phys 374:4919–4927. https://doi.org/10.1016/j.physleta.2010.10.014

Zhong DK, Choi S, Gamelin DR (2011) Near-complete suppression of surface recombination in solar photoelectrolysis by "Co-Pi" catalyst-modified W:BiVO4. J Am Chem Soc 133: 18370–18377. https://doi.org/10.1021/ja207348x

Zhou B, Qu J, Zhao X, Liu H (2011) Fabrication and photoelectrocatalytic properties of nanocrystalline monoclinic $BiVO_4$ thin-film electrode. J Environ Sci 23:151–159. https://doi.org/10.1016/S1001-0742(10)60387-7

Zhou L, Wang W, Liu S, Zhang L, Xu H, Zhu W (2006) A sonochemical route to visible-light-driven high-activity $BiVO_4$ photocatalyst. J Mol Catal A Chem 252:120–124. https://doi.org/10.1016/j.molcata.2006.01.052

Zhu Z, Zhang L, Li J, du J, Zhang Y, Zhou J (2013) Synthesis and photocatalytic behavior of $BiVO_4$ with decahedral structure. Ceram Int 39:7461–7465. https://doi.org/10.1016/j.ceramint.2013.02.093